



Article

Differential Effects of Lipid Bilayers on α PSM Peptide Functional Amyloid Formation

Kamilla Kristoffersen, Kasper Holst Hansen and Maria Andreassen * 

Department of Biomedicine, Aarhus University, Willhelm Meyer's Allé 3, 8000 Aarhus, Denmark

* Correspondence: mariaj@biomed.au.dk

Abstract: Phenol-soluble modulins (PSMs) are key virulence factors of *S. aureus*, and they comprise the structural scaffold of biofilm as they self-assemble into functional amyloids. They have been shown to interact with cell membranes as they display toxicity towards human cells through cell lysis, with α PSM3 being the most cytotoxic. In addition to causing cell lysis in mammalian cells, PSMs have also been shown to interact with bacterial cell membranes through antimicrobial effects. Here, we present a study on the effects of lipid bilayers on the aggregation mechanism of α PSM using chemical kinetics to study the effects of lipid vesicles on the aggregation kinetics and using circular dichroism (CD) spectroscopy, Fourier-transform infrared (FTIR) spectroscopy and transmission electron microscopy (TEM) to investigate the corresponding secondary structure of the aggregates. We found that the effects of lipid bilayers on α PSM aggregation were not homogeneous between lipid type and α PSM peptides, although none of the lipids caused changes in the dominating aggregation mechanism. In the case of α PSM3, all types of lipids slowed down aggregation to a varying degree, with 1,2-dioleoyl-sn-glycero-3-phosphocholine (DOPC) having the most pronounced effect. For α PSM1, lipids had opposite effects, where DOPC decelerated aggregation and lipopolysaccharide (LPS) accelerated the aggregation, while 1,2-dioleoyl-sn-glycero-3-phospho-rac-(1-glycerol) (DOPG) had no effect. For α PSM4, both DOPG and LPS accelerated the aggregation, but only at high concentration, while DOPC showed no effect. None of the lipids was capable of inducing aggregation of α PSM2. Our data reveal a complex interaction pattern between PSMs peptides and lipid bilayers that causes changes in the aggregation kinetics by affecting different kinetic parameters along with only subtle changes in morphology.

Keywords: phenol-soluble modulins; functional amyloids; protein aggregation; protein–lipid interactions; lipid vesicles



Citation: Kristoffersen, K.; Hansen, K.H.; Andreassen, M. Differential Effects of Lipid Bilayers on α PSM Peptide Functional Amyloid Formation. *Int. J. Mol. Sci.* **2024**, *25*, 102. <https://doi.org/10.3390/ijms25010102>

Academic Editors: Alessandra Piscitelli and Paola Cicatiello

Received: 3 November 2023

Revised: 16 December 2023

Accepted: 17 December 2023

Published: 20 December 2023



Copyright: © 2023 by the authors. Licensee MDPI, Basel, Switzerland. This article is an open access article distributed under the terms and conditions of the Creative Commons Attribution (CC BY) license (<https://creativecommons.org/licenses/by/4.0/>).

1. Introduction

Functional amyloids are found in a wide variety of organisms in nature, where they provide a variety of functionalities ranging from storage of peptide hormones [1] to melanin granula formation [2] to virulence during infection [3] to forming scaffolds during biofilm formation [4,5]. Functional bacterial amyloids are secreted from bacteria as components of the biofilm, where they normally assemble into β -sheet-rich fibrils [6], providing stability to the biofilm [7]. In *S. aureus*, the functional amyloids are formed from small amphipathic peptides called phenol-soluble modulins (PSMs) [8]. Among other things, PSMs act as a structural scaffold in the biofilm matrix, increasing antibiotic resistance and biofilm integrity [9,10]. *S. aureus* produces seven PSMs called α PSM1–4, β PSM1–2 and δ -toxin [8]. The four α -group peptides consist of ~20 amino acids, and the two β -group peptides consist of ~40 amino acids [8]. α PSM1 and α PSM4 form prototypical amyloid fibrils which exhibit the typical cross- β structural signature, although with a great deal of structural polymorphism [11]. On the other hand, α PSM3 fibrils display a unique cross- α structure [12–14]. This structure enhances α PSM3 toxicity against human cells [15].

In addition to biofilm formation, the monomeric soluble PSM peptides have multiple functions including proinflammatory activity, cytotoxic activity by lysis of erythrocytes and neutrophils and antimicrobial activity [8,16–20]. In addition to in functional amyloid formation, α PSMs are also abundant on the cell surface, and expression of α PSMs on the cell surface of *S. aureus* promotes colony spreading [21]. Furthermore, community-associated methicillin-resistant *S. aureus* (CA-MRSA) has an extraordinary capacity to avoid being killed by neutrophils of the human innate immune system, even after phagocytosis by the neutrophils [22], and, additionally, PSMs contribute to phagosomal escape and intracellular lysis of the neutrophils [17,23]. The capacity to lyse human neutrophils is almost entirely dependent on the expression of PSM α genes [8]. The cytolytic activity of the PSM peptides differs, with α PSM3 displaying high cytolytic activity [24] and α PSM1 and α PSM2 only showing moderate activity and α PSM4 showing none [12,25]. Fibrillation, along with positive charges, plays a central role in α PSM3 cytolytic activity [14]. Unprocessed PSM peptides do not elicit antimicrobial activity in CA-MRSA [19]. Research shows that α PSM3 derivatives without large hydrophobic side chains elicit moderate-to-strong antimicrobial activity [26].

The complexity of functional amyloid formation in bacterial biofilms is increased by interactions between amyloid proteins and other components such as lipids, other proteins, nucleic acids and metal ions present in the biofilm [27]. Lipoproteins in human serum have the ability to inhibit PSM-induced lysis of neutrophils, with high-density lipoprotein (HDL) being the most potent one [28,29]. Cholesterol in the membrane (between 10 and 30 mol%) increases the lytic activity of α PSM1–4, and the ability of PSMs to form an α -helical structure is important for lysing cholesterol containing lipid vesicles [16]. Lipids have also been shown to affect other functional amyloid systems. The aggregation of curli-forming proteins CsgA and CsgB in *E. coli* is highly accelerated by the presence of lipopolysaccharide (LPS) [30], and the aggregation of FapC from *Pseudomonas* is also accelerated in terms of both increased growth rate and decreased lag phase in the presence of LPS [31]. The self-assembly of other amyloid proteins associated with pathology is also affected by the presence of various lipids. α -synuclein, involved in Parkinson's disease pathology, has been shown to bind to lipid model membranes, resulting in a significant increase in aggregation rate, specifically the primary nucleation rate [32], and further investigation has shown that α -synuclein transitions from coil to α -helix when in contact with lipid bilayers [33]. Thus, lipid interactions with amyloid-forming peptides or proteins have been investigated multiple times in different settings, showing a connection between the two.

This notion makes it interesting to further investigate the interaction between lipid bilayers and PSM peptides since α PSM3 peptides have been shown to aggregate on the cell membranes, leading to membrane rupture and cell death [14]. Here, we investigated how different lipids could impact the aggregation of all the α PSM peptides. Since PSMs have antimicrobial activity [19], we additionally examined whether components in bacterial cell membranes affected the aggregation of PSMs.

2. Results

2.1. Chemical Kinetics Reveal Variation in Aggregation Rates for α PSM Peptides in the Presence of Different Lipids

To investigate the effect of lipids on the aggregation of α PSM peptides, we incubated peptides individually at fixed monomeric concentrations with varying concentrations of lipids. Aggregation kinetics were monitored using the amyloid-binding dye thioflavin T (ThT) [34]. We used lipid vesicles containing different lipids, namely, the zwitterionic 1,2-dioleoyl-sn-glycero-3-phosphocholine (DOPC) and the negatively charged 1,2-dioleoyl-sn-glycero-3-phospho-rac-(1-glycerol) (DOPG), and lipid vesicles mimicking bacterial cell membranes consisting of lipopolysaccharide (LPS) from Gram-negative bacteria and L- α -phosphatidylethanolamine (PE) with various fatty acid chains extracted from *E. coli*. All lipids were processed to mimic the lipid bilayer structure of cell membranes by forming

unilamellar vesicles of uniform size. Peptide concentrations were chosen in accordance with previous PSM studies on aggregation in the absence of lipids [35].

For α PSM1, α PSM3 and α PSM4, reproducible aggregation curves were observed in the presence of DOPC, DOPG and LPS lipids (Figure 1). The presence of the lipid vesicles did not affect the ThT signal of α PSM peptide aggregates (Figure S1d–f). A linear scaling of the end ThT fluorescence signal with respect to the monomer peptide concentration was seen for α PSM1, α PSM3 and α PSM4 (Figure S1a–c). Kinetic data are thus presented as normalized ThT fluorescence curves with the y-axis converted to relative aggregate concentration. In the case of α PSM2, no aggregation occurred with any of the lipids (Figure S2d–f). A summation of lipid effect on α PSMs is shown in Table 1.

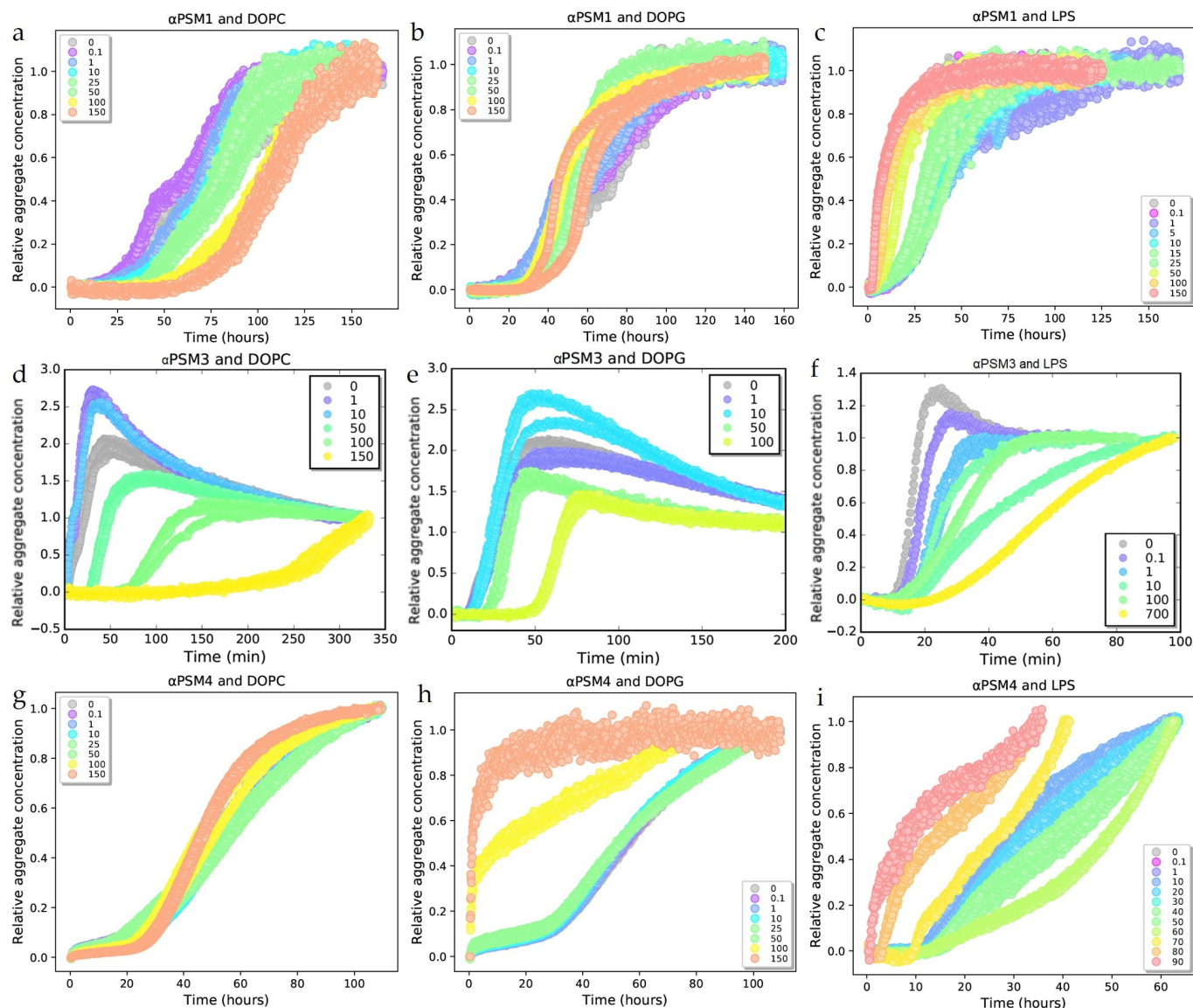


Figure 1. Experimental kinetic data for the aggregation of phenol-soluble modulins (PSM) peptides combined with lipids. Data are represented as normalized fluorescence curves. (a) Aggregation of α PSM1 (0.5 mg/mL) in the presence of DOPC lipid in different concentrations (0–150 μ g/mL). (b) Aggregation of α PSM1 (0.5 mg/mL) in the presence of added DOPG lipid in different concentrations (0–150 μ g/mL). (c) Aggregation of α PSM1 (0.5 mg/mL) in the presence of LPS lipid in different concentrations (0–150 μ g/mL). (d) Aggregation of α PSM3 (0.5 mg/mL) in the presence of DOPC lipid in different concentrations (0–150 μ g/mL). (e) Aggregation of α PSM3 (0.5 mg/mL) in the presence of DOPG lipid in different concentrations (0–100 μ g/mL). (f) Aggregation of α PSM3 (0.5 mg/mL) in the

presence of LPS lipid in different concentrations (0–700 $\mu\text{g/mL}$). (g) Aggregation of αPSM4 (0.25 mg/mL) in the presence of DOPC lipid in different concentrations (0–150 $\mu\text{g/mL}$). (h) Aggregation of αPSM4 (0.25 mg/mL) in the presence of DOPG lipid in different concentrations (0–150 $\mu\text{g/mL}$). (i) Aggregation of αPSM4 (0.25 mg/mL) in the presence of LPS lipid in different concentrations (0–90 $\mu\text{g/mL}$). All kinetic experiments were carried out in triplicates.

Table 1. Summation of lipid vesicles' effect on aggregation for αPSM peptides. \uparrow : Acceleration of aggregation kinetics, \downarrow : Deceleration of aggregation kinetics.

αPSM	DOPC	DOPG	LPS
αPSM1	\downarrow	-	\uparrow
αPSM3	\downarrow	\downarrow	\downarrow
αPSM4	-	\uparrow	\uparrow

The aggregation kinetics for αPSM1 did not significantly change when DOPG lipid vesicles were added (Figure 1b). However, changes in aggregation kinetics occurred when either DOPC or LPS vesicles were added to αPSM1 . The aggregation rate decreased with higher DOPC concentrations, increasing the lag phase from ~ 25 h to ~ 50 h in a dose-dependent manner (Figure 1a). Interestingly, LPS vesicles had the opposite effect on the aggregation kinetics of αPSM1 , and the aggregation was hence accelerated in a dose-dependent manner. At higher LPS concentrations (100–150 $\mu\text{g/mL}$), the lag phase was only ~ 2 h; therefore, the plateau was reached within ~ 25 h compared to ~ 40 h for the αPSM1 control sample in the absence of lipid vesicles (Figure 1c). The effect of lipids on the aggregation half-time can be seen in Figure S3.

The aggregation kinetics of αPSM3 were highly affected by the addition of lipid vesicles. Higher concentrations of all three lipids (DOPC, DOPG and LPS) all decelerated the aggregation kinetics of αPSM3 , with DOPC lipid vesicles having the most profound effect. At higher concentrations of DOPC lipid vesicles, the lag phase was increased from ~ 10 min to ~ 250 min (Figure 1d). In the absence of lipid, the plateau phase was reached after ~ 50 min. This was increased to ~ 80 min with high concentrations of DOPG (Figure 1e), ~ 100 min with high concentrations of LPS (Figure 1f) and, with high concentrations of DOPC, the plateau phase was not reached even after ~ 320 min (Figure 1d). The deceleration of the aggregation kinetics of αPSM3 by addition of lipids was further confirmed by the increase in aggregation half-time as a function of lipid concentration (Figure S3d–f), further confirming that DOPC lipid vesicles have the biggest effect on the aggregation kinetics of αPSM3 .

In the presence of DOPC lipid vesicles, the aggregation kinetics for αPSM4 did not show any significant changes (Figure 1g). This behavior was also seen for LPS and DOPG lipid vesicles at low concentration, with no significant changes seen in the aggregation kinetics of αPSM4 . However, at high concentrations of DOPG (100–150 $\mu\text{g/mL}$), the aggregation kinetics of αPSM4 appeared to be almost seeded as the lag phase disappeared (Figure 1h). In the presence of high concentrations of LPS lipid vesicles (80–90 $\mu\text{g/mL}$), the lag phase was still present but significantly shorter at 0–1 h compared to ~ 15 h for the control αPSM4 sample in the absence of lipids. The highest concentration of LPS lipids also caused the aggregation kinetics to appear to be seeded (Figure 1i).

In addition to DOPC, DOPG and LPS lipid vesicles kinetic experiments were also conducted with vesicles of PE lipids extracted from *E. coli* membranes to test whether lipids found in the outer leaflet of bacterial cell membranes could influence the aggregation of αPSM peptides. PE lipid vesicles had no effect on the aggregation of αPSM4 , while aggregation of αPSM3 was completely inhibited by the presence of PE lipid vesicles. αPSM1 aggregation kinetics were slower in the presence of PE lipid vesicles; however, the aggregation kinetics in the presence of PE became un-reproducible, and single curves in a triplicate no longer followed the same trend. For these reasons, the aggregation in the presence of PE lipid vesicles was not further examined (Figure S2a–c).

The differences in the lag phases between control samples of the same peptides were ascribed to batch-to-batch variations from the manufacturer, a phenomenon which has been observed before for synthetic peptides [36].

2.2. Fitting of ThT Curves Using Amylofit Reveals Different Mechanisms of Fibril Kinetics

To establish how the different lipids affected the molecular steps of aggregation in α PSM peptides, we used chemical kinetics to analyze the aggregation [37]. Kinetic models of protein aggregation have previously been applied for different model systems of protein aggregation [35,38–40]. Through the analysis of rates and reaction orders of underlying molecular events, the kinetic analysis of aggregation data renders it possible to determine the dominating molecular mechanism by which new aggregates are formed. We have previously shown that all α PSM peptides aggregate through a secondary-nucleation-dominated mechanism [35]. Kinetic parameters from this previous analysis of the aggregation of α PSMs in the absence of lipids were used as fixed global parameters where only one compound rate constant was individually fitted to the lipid concentration, either $k_n k_+$ or $k_+ k_2$, with k_n being the rate constant of primary nucleation, k_+ being the rate constant of elongation and k_2 being the rate constant of secondary nucleation. This approach has previously been used to establish how inhibitors influence specific microscopic steps during aggregation of other amyloidogenic proteins [41–43]. In some cases, a global fit for one of the compound rates, in addition to the compound rates allowed to vary with lipid concentration, was used to get a decent fit. A similar approach has previously been used to investigate the effect of heparin on the aggregation of PSM peptides [44]. The presence of lipids did not alter the dominating aggregation mechanism for any of the peptides, and all α PSM peptides were successfully fitted to a secondary-nucleation-dominated aggregation mechanism. The addition of heparin to β PSM2 has been observed to change the dominating aggregation mechanism from nucleation elongation dominated to secondary nucleation dominated. Fits to kinetic data are shown in Figure S4, and results from these fits are provided in Table S1.

For α PSM1 and DOPC lipid vesicles, the best fits were obtained by allowing $k_+ k_2$ to vary with every lipid concentration while $k_+ k_n$ was fitted as a global constant to all concentrations. The values of n_c (reaction order of the primary nucleation) and n_2 (reaction order of the secondary nucleation) were restricted to the control lipid-free values (Figure S4a). Since both compound rates needed to differentiate from the control lipid-free kinetics, it is very likely that both k_+ and k_2 were affected by the presence of DOPC lipid vesicles. Interestingly, $\log(k_+ k_2)$ values for the fit decreased in a linear fashion when plotted against the DOPC concentration (Figure 2a). When plotting the log of unfolding rates versus the concentration of denaturants or surfactant, similar linear relationships are found [45,46]. Since the concentration of the lipid was low (0.1 to 150 $\mu\text{g/mL}$), the interactions between the lipid and the PSM peptides were clearly strong in contrast to what is seen for denaturants which are used at high concentrations, indicating that the interactions occurring with proteins are driven by weak forces. The presence of DOPG lipid vesicles did not have a clear effect on the aggregation kinetics of α PSM1 (Figure 1b), which was further confirmed by the lack of a trend in the half-time plot (Figure S3b). During the kinetic fitting analysis, the best fit was found by varying the $k_+ k_2$ compound rate constant while globally fitting the $k_n k_+$ compound rate constant. The other kinetic parameters (n_c and n_2) were restricted to the lipid-free control values (Table S1). This indicates that the rate constant which is affected by DOPG lipid vesicles is k_+ , although the changes are small, as also indicated by the small changes in $k_+ k_2$ with lipid concentration (from 14.9 in the absence of lipids to 26.4 at the highest concentration of lipids, Table S1). The obtained $k_+ k_2$ compound rates can be fitted to a linear line in a log–log plot, although the R^2 value ($R^2 = 0.69$) further indicates a rather poor linear fit (Figure 2b). For α PSM1 and LPS, the best fit was obtained when $k_+ k_2$ was varied with every lipid concentration and $k_+ k_n$, n_c and n_2 were restricted to the lipid-free control values. This indicates that k_2 is the rate constant affected the most since changes in k_+ would also lead to changes in the second compound rate constant

$k_n k_2$. A linear increase was seen when $\log(k_+ k_2)$ was plotted against the LPS concentration, similarly to what was seen for DOPC and α PSM4 (Figure 2c,g).

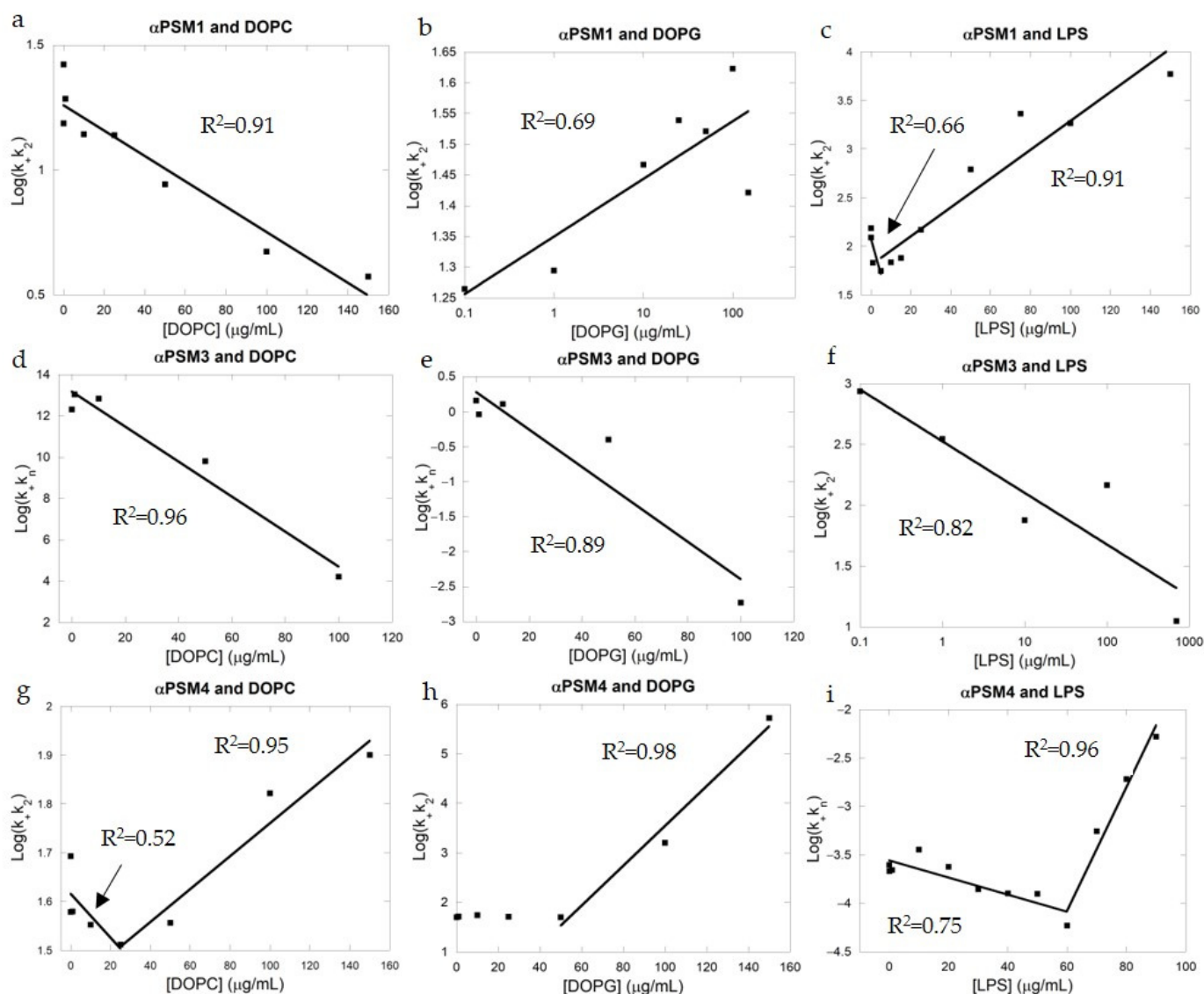


Figure 2. Plots of different composite rate constants obtained from fits to PSM aggregation data versus lipid concentration. (a) α PSM1 and DOPC. (b) α PSM1 and DOPG. (c) α PSM1 and LPS. (d) α PSM3 and DOPC. (e) α PSM3 and DOPG. (f) α PSM3 and LPS. (g) α PSM4 and DOPC. (h) α PSM4 and DOPG. (i) α PSM4 and LPS. The R^2 of the linear fit to the data points (black squares) is given in each plot.

For the kinetic data of α PSM3 and DOPC lipid vesicles, the best fit was found when $k_+ k_n$ was allowed to vary with lipid concentration (Figure 2d). To obtain the best possible fit, n_c and n_2 values were also required to differ from the lipid-free control values. The values for n_c and n_2 used for the fit were found through trial by fitting of each parameter individually. Ultimately, n_c , n_2 and $k_+ k_2$ were kept as global constants, meaning that k_n is the parameter most affected by the presence of DOPC lipid vesicles. This is also apparent from the kinetic curves, where the lag phase is clearly lengthened by additions of lipids; hence, DOPC vesicles clearly influence the primary nucleation of α PSM3. DOPG lipid vesicles also delay the aggregation kinetics of α PSM3, and the kinetic data were fitted with $k_+ k_n$ varying with lipid concentration. Additionally, the $k_+ k_2$ compound rate constant also needed to be a global fit, along with n_c , to obtain a good fit to the kinetic data. This indicates that both the primary nucleation and the elongation are altered in the presence

of DOPG lipid vesicles. The decrease in the $\log(k_+k_n)$ followed a linear trend for α PSM3 in the presence of both DOPC and DOPG lipid vesicles (Figure 2d,e). For α PSM3 and DOPG kinetic data fitting, the k_+k_n varied with lipid concentration, leaving k_+k_2 as a global fitted parameter and n_c and n_2 as constant values. For α PSM3 and LPS, k_+k_2 was a fitted parameter with every concentration, leaving k_+k_n as a global fitted parameter and the lipid-free control parameters of n_c and n_2 as constant values. Since both compound rate constants were different from the lipid-free control values, it indicates that the parameter k_+ is affected by the presence of LPS lipid vesicles. This is also apparent from the kinetic data where the slope of the elongation phase clearly changes with increasing lipid concentration. The decrease in k_+k_2 follows a linear pattern in a log–log plot when plotted against the lipid concentration (Figure 2f). Log–log patterns like this are similarly observed for ligand-binding systems, with a strong specific interaction between the ligand and the protein indicating a strong specific interaction between LPS lipid vesicles and α PSM3.

For all cases of kinetic data fitting to α PSM4 in the presence of lipids, bi-phasic behavior is seen with low concentration of lipids, giving either a small decrease in the kinetic compound rate constant or no changes at all. This is followed by an increase in the kinetic parameter at high concentrations of lipids regardless of the lipid. For α PSM4, the best fits for DOPC and DOPG were found when k_+k_2 varied with lipid concentration and the rest of the parameters were kept constant using the lipid-free control values (Figure S4g,h). For α PSM4 and LPS, the best fit was found when k_+k_n was left to vary with lipid concentration and the rest were constant lipid-free control parameters (Figure S4i). $\log(k_+k_2)$ plotted against the concentrations of DOPC and DOPG reveals a bipartite graph initially with a decreasing (DOPC) or linear (DOPG) manner changing to an increasing linear pattern (Figure 2g,h). In the presence of LPS lipids, the $\log(k_nk_+)$ plot is bipartite, starting with a negative slope that turns into a positive slope at 60 $\mu\text{g/mL}$ LPS (Figure 2i).

2.3. Lipids Have Modest Effects on the Secondary Structure of PSM Fibrils

To address whether adding lipids affected the secondary structure of the fibrillar aggregates of α PSM peptide, we used circular dichroism (CD) and Fourier-transform infrared (FTIR) spectroscopy. Individual CD spectra are shown in Figure 3a–i, and individual FTIR spectra are presented in Figure S5a–i. Deconvolution of FTIR results is shown in Figure 4a–c.

α PSM1 has previously been shown to form β -sheet-rich fibrils [11,35], and smaller fragments of α PSM1 have shown polymorphism but with all fibril polymorphs being rich in β -sheet structures. For α PSM1, we also observed β -sheet-rich fibril structures based on the single minima at 219 nm in CD, indicative of a β -sheet structure, and, from the deconvolution of the FTIR data, more than 65% of the structure contribution was from β -sheets and β -turns. CD data and FTIR showed no changes in samples with α PSM1 and DOPG, which corresponds to the kinetic data where no significant changes occurred in the presence of DOPG lipid vesicles (Figures 3a and 4a). FTIR of α PSM1 showed a slight change in the secondary structure of the fibrils when DOPC was added in a low concentration; however, no changes in structure were found at high concentrations of DOPC (Figure 4a). For α PSM1 and DOPC, the CD signal changed intensity, corresponding with the kinetic data which showed slower aggregation, which may have resulted in fewer fibrils being formed at the end stage of aggregation, resulting in a signal decrease in CD (Figure 3a). Alternatively, the decrease in signal intensity could also have been caused by the formation of fibrils with altered structures. LPS, on the other hand, accelerated the aggregation kinetics of α PSM1, and CD data showed a higher signal in samples with higher LPS concentration but with no changes to the wavelength of the minimum observed (Figure 3c). FTIR data showed an enrichment of the β -sheet structure of α PSM1 fibrils at low concentrations of LPS (Figure 4a).

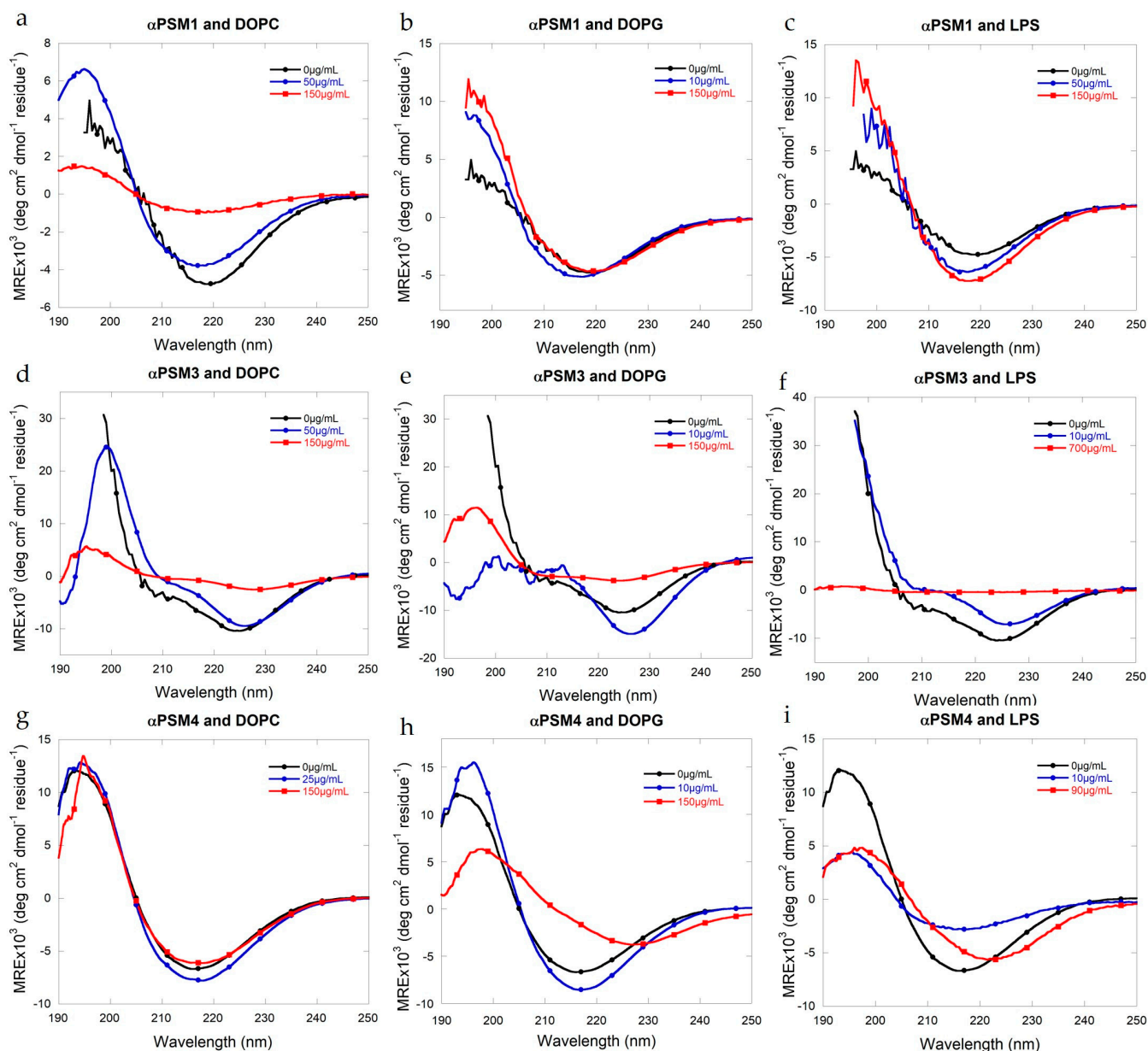


Figure 3. Structural comparison of fibrils formed by α PSM peptides when lipid vesicles are added. (a) Far-UV CD spectra for α PSM1 with added DOPC. (b) Far-UV CD spectra for α PSM1 with added DOPG. (c) Far-UV CD spectra for α PSM1 with added LPS. (d) Far-UV CD spectra for α PSM3 with added DOPC. (e) Far-UV CD spectra for α PSM3 with added DOPG. (f) Far-UV CD spectra for α PSM3 with added LPS. (g) Far-UV CD spectra for α PSM4 with added DOPC. (h) Far-UV CD spectra for α PSM1 with added DOPG. (i) Far-UV CD spectra for α PSM4 with added LPS.

The α PSM3 control sample aggregate showed a cross- α -helical structure consistent with previous studies [14,15]. For α PSM3, the CD spectra changed drastically for fibrils in the presence of all three lipids, and the changes were more pronounced with higher lipid concentration (Figure 3d,f). The signal intensity decreased, and the double minima signature of the signal indicates that the α -helical structure was less pronounced. Additionally, the minimum changed from 224 nm to 227.8 nm (Table S2) for α PSM3 with a high concentration of DOPC (Figure 3d) and from 224 nm to 213.5 nm (Table S2) for α PSM3 with a high concentration of LPS (Figure 3f). The minima changes correlated well with the FTIR data, which showed that the fibril of α PSM3 in the presence of all three lipids displays more β -sheet-rich structures (Figure 4b). For α PSM3 and DOPG, FTIR data revealed a complete

change in structure as there was almost no α -helix left with the high concentration of DOPG (Figure 4b). For all three lipid samples, the signal intensity decreased, with higher lipid concentrations corresponding with the kinetic data where the aggregation was decelerated when adding lipids.

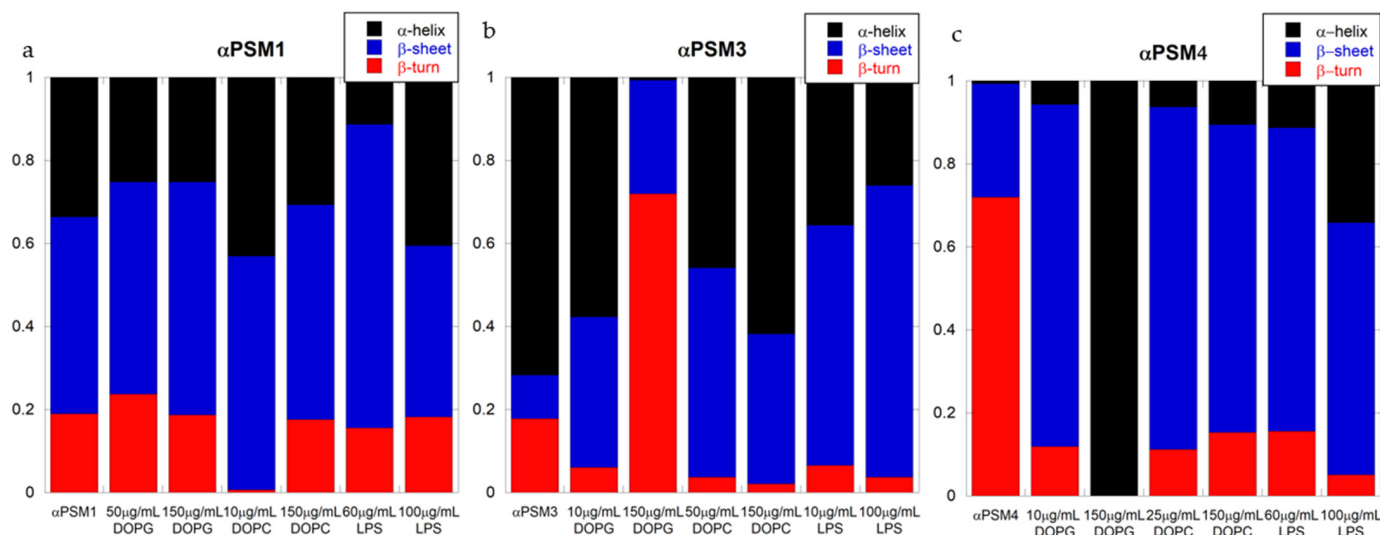


Figure 4. Deconvolution of the FTIR spectra of fibrils of the PSM peptides in the absence and presence of lipid vesicles. (a) PSM α 1 with DOPG, DOPC and LPS at high and low concentrations. (b) PSM α 3 with DOPG, DOPC and LPS at high and low concentrations. (c) PSM α 4 with DOPG, DOPC and LPS at high and low concentrations.

For α PSM4, the CD spectra showed no changes when DOPC was added (Figure 3g), which corresponds with the kinetic data where no significant changes in the kinetic curves were seen when DOPC lipid vesicles were added (Figure 1g). However, the FTIR data with DOPC showed a shift from β -sheets to β -turns at low concentrations of DOPC when compared to the lipid-free control sample (Figure 4c); this was also the case when LPS was added. For α PSM4, a change in secondary structure was seen when combined with either DOPG or LPS. The minimum was red shifted from 216 nm to 226.9 nm (Table S2) for α PSM4 with added DOPG (Figure 3h) and to 222.5 nm when LPS was added (Figure 3i and Table S2). The change in the minimum for α PSM4 with DOPG correlates well with the FTIR data, which showed a complete change to the α -helix only (Figure 4c). Interestingly, the CD signal intensity went down when the concentration of lipid went up, even though the kinetics showed a faster aggregation. This could indicate that, although the aggregation kinetics were accelerated, the amount of aggregated sample was less in the presence of high concentrations of DOPG.

2.4. Morphology Shows Fibril Formation When Adding Lipids to α PSM Peptides

The morphological features of aggregates from α PSM peptides with and without lipid were analyzed by transmission electron microscopy (TEM). Morphology of PSMs with low lipid concentration is shown in Figure S6. After incubation, α PSM1 formed long, entangled, amyloid-like fibrils, similar to what has been observed for α PSM1 previously [35] (Figure 5a). When 150 μ g/mL of DOPC was added, we still saw entangled fibrils forming a network; however, the fibrils appeared shortened, and the network was less dense, consistent with the aggregation kinetics which are delayed in the presence of DOPC lipid vesicles. Lipid vesicles are also apparent in the images as a blur entangled with the fibrils (Figure 5b). In some areas where α PSM1 and DOPC were combined, large deposits of lipids were seen, and the morphology of the fibrils differed since the aggregates appeared decorated by amorphous aggregates (Figure S7a,b). Despite no significant effect on the aggregation kinetics, adding 150 μ g/mL of DOPG to α PSM1 resulted in a shortening of

the fibrils along with the occurrence of less network structure, hence changing the fibril morphology despite similar aggregation kinetics. In some areas, lipids were observed occurring like a blur with aggregates close by (Figure 5c). Adding 100 $\mu\text{g}/\text{mL}$ LPS to αPSM1 changed the fibril structure. The fibrils became shorter and thinner, and, in areas, the fibrils were combined with the LPS in larger structures where it was hard to establish the structure of individual fibrils (Figure 5d). αPSM3 generated shorter, ribbon-like and unbranched fibrils (Figure 5e), consistent with the morphology previously reported [35]. DOPC changed the number of fibrils seen in the TEM images. This correlates with the kinetic results, where DOPC was observed to have the largest impact by decelerating the aggregation to the largest extent. Furthermore, lipids were observed on the surface of the fibrils (Figure 5f). Although DOPG and LPS both decelerated the aggregation kinetics, the effect was less pronounced than in the presence of DOPC. This is also reflected in the TEM images, where significantly more aggregates were observed on the TEM grids for samples with DOPG and LPS compared to DOPC. In the presence of DOPG lipid vesicles, the αPSM3 aggregate morphology resembles the lipid-free control samples (Figure 5g). αPSM3 with 100 $\mu\text{g}/\text{mL}$ LPS also resulted in fibrils resembling the control samples; however, LPS could be seen to associate with the fibrils (Figure 5h).

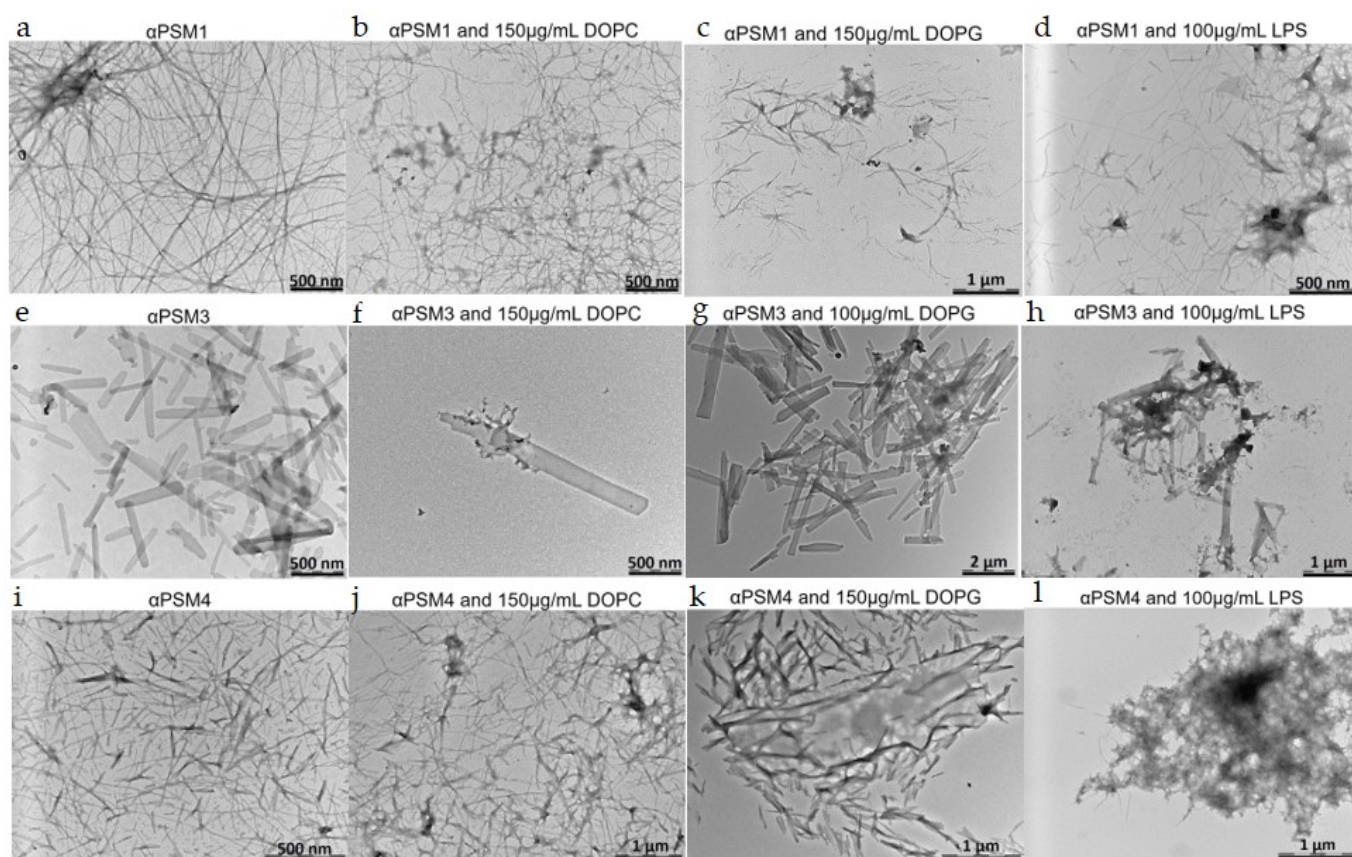


Figure 5. Morphology of aggregates of αPSM peptides with and without lipids. Transmission electron microscopic image of the end-state fibril of αPSM peptides in the absence and presence of DOPC, DOPG and LPS lipid vesicles. (a) αPSM1 fibrils. (b) αPSM1 with 150 $\mu\text{g}/\text{mL}$ DOPC. (c) αPSM1 with 150 $\mu\text{g}/\text{mL}$ DOPG. (d) αPSM1 with 100 $\mu\text{g}/\text{mL}$ LPS. (e) αPSM3 fibrils. (f) αPSM3 with 150 $\mu\text{g}/\text{mL}$ DOPC. (g) αPSM3 with 100 $\mu\text{g}/\text{mL}$ DOPG. (h) αPSM3 with 100 $\mu\text{g}/\text{mL}$ LPS. (i) αPSM4 fibrils. (j) αPSM4 with 150 $\mu\text{g}/\text{mL}$ DOPC. (k) αPSM4 with 150 $\mu\text{g}/\text{mL}$ DOPG. (l) αPSM4 with 100 $\mu\text{g}/\text{mL}$ LPS.

In the absence of lipid vesicles, αPSM4 formed fibrils with a morphology different from what has been reported for αPSM4 previously. The fibrils were shorter and thicker than in previous reports of αPSM4 (Figure 5i). When DOPC was added, the fibrils appeared

thinner, and the network of aggregates was less dense (Figure 5j). DOPG lipid vesicles caused the α PSM4 fibrils to become even shorter, and there appeared to be lipid embedded in the fibril formation (Figure 5k). Despite the accelerated aggregation observed for high concentrations of LPS lipid vesicles, very few fibril structures were observed. The few fibrils present appeared to branch out from larger amorphous structures, and no fibril network was seen (Figure 5l).

3. Discussion

We studied the aggregation of α PSMs from *S. aureus* in the presence of single lipid vesicles, namely, DOPC, DOPG, lipopolysaccharide (LPS) from Gram-negative bacteria and PE from *E. coli*, using kinetic data and chemical kinetic analysis combined with secondary structure analysis using CD and FTIR and morphological analysis using TEM. Kinetic analysis revealed a varied effect of adding lipid to the PSM peptides; however, the effects were not homogenous between peptides and lipids. Analysis of the secondary structures revealed structural changes in agreement with the effects observed from the kinetic data.

In the *E. coli* curli system, LPS, found in the outer leaflet of Gram-negative bacterial cells [47], increases the rate of aggregation of CsgA and CsgB as a function of LPS concentrations [30]. We examined whether membrane lipids from bacteria could impact aggregation of α PSMs. The membrane lipid PE from *E. coli* did not accelerate aggregation of any of the α PSM peptides; in fact, PE blocked aggregation of α PSM3 all together (Figure S2b). Hence, lipids from the membrane of bacteria are not able to aid in functional amyloid formation. This is the opposite effect to what is observed with respect to the LPS membrane component in the *E. coli* CsgA and CsgB system. The lack of effect from lipids from the bacterial membrane could possibly originate from the thick peptidoglycan layer found in Gram-positive bacteria [48]. This peptidoglycan layer could block the lipid surface from molecules found in the biofilm, and, hence, the bacteria might not benefit from accelerated aggregation of PSM peptides immediately adjacent to the cell membrane. Interestingly, LPS from the outer membrane of Gram-negative bacteria does influence aggregation when added to α PSM peptides. LPS accelerates the aggregation of both α PSM1 and α PSM4 but slows down aggregation of α PSM3. It is hard to determine whether the altered aggregation kinetics of α PSM3 are linked to the reported antimicrobial activity of α PSM3 [19] or whether other properties, e.g., structural properties such as the cross- α fibril structure, play a part [15].

It has previously been shown that the cytotoxicity effect of α PSM3 is promoted by aggregation and by introduction of positive charges in the amino acid sequence [14]. This could suggest that interaction between α PSM3 and negatively charged phospholipids would be favorable due to static attraction. However, the aggregation results in this study show that the charge of the lipids does not affect the fibrillation. All α PSM peptides have a net positive charge at neutral pH (isoelectric point (pI): α PSM1 = 9.7, α PSM2 = 10, α PSM3 = 9.5 and α PSM4 = 9.7), but all the peptides respond differently to the presence of the negatively charged DOPG lipid vesicles. No aggregation was induced for α PSM2, no changes in aggregation kinetics were seen for α PSM1, aggregation was decelerated for α PSM3 and aggregation was accelerated for α PSM4 in the presence of DOPG lipid vesicles (Figure 1). Furthermore, all other lipid tested here were zwitterionic, and they also elicited different responses from the peptides in terms of changes in the aggregation kinetics. Hence, our results show that the changes in aggregation kinetics in the presence of lipids are not governed by charges.

It has previously been showed that α PSM3 interacts with lipid bilayers in a species-specific manner, resulting in increased cytolytic activity for membranes mimicking mammalian cells [49]. It was furthermore reported that aggregation of α PSM3 was accelerated in the presence of lipid bilayers. Our current study shows aggregation of α PSM3 was slowed down with all lipids tested in a dose-dependent manner (Figure 1d–f). This is not in correlation with previous findings. However, different lipid compositions were used here; we used one single lipid for each system, compared to previous studies, where a

mixture of lipids was used [49]. These differences in lipid composition could have led to the different effects observed here and in previous studies. Furthermore, in the previous studies, cholesterol was included in the lipid mixtures, and cholesterol clearly affects the PSM–lipid interaction [16]. Another explanation for the slower aggregation kinetics in our study could be the peptide–lipid interaction on the surface of the lipid vesicles leading to sequestration of peptide molecules to the lipid surface. This would lower the effective peptide concentration in solution.

The presence of the lipids in the current study did not induce aggregation of α PSM2. In normal in vitro conditions, α PSM2 does not aggregate by itself in aqueous solutions [35], and previous studies with heparin also failed in inducing aggregation of α PSM2 [44]. For α PSM3, aggregation promoted the cytolytic activity [12]; however, since α PSM2 has reported cytolytic activity but aggregation is not induced in the presence of lipid bilayers, the cytolytic activity of α PSM2 seems to be independent from aggregation. Interestingly, this seems to be the opposite effect for α PSM4. No cytolytic activity is reported for α PSM4, but we observed an acceleration of aggregation in the presence of high concentrations of DOPC and LPS lipids. Hence, no direct line can be drawn between the ability to lyse mammalian cells and aggregation of α PSM peptides.

4. Materials and Methods

4.1. Peptides and Reagents

N-terminally formylated peptides (>95% purity) were purchased from Genscript Biotech, Rijswijk, The Netherlands. Hexafluoroisopropanol (HFIP), thioflavin T (ThT), lipopolysaccharide (LPS) from Gram-negative bacteria and trifluoroacetic acid (TFA) were purchased from Sigma Aldrich, St. Louis, MO, USA. Dimethyl sulfoxide (DMSO) was purchased from Merck, Darmstadt, Germany. 1,2-dioleoyl-sn-glycero-3-phosphocholine (DOPC), 1,2-dioleoyl-sn-glycero-3-phospho-rac-(1-glycerol) (DOPG), L- α -phosphatidylethanolamine (PE) extracted from *E. coli*, extrusion filters and filter supports were purchased from Avanti Polar Lipids, Birmingham, AL, USA.

4.2. Preparation of Synthetic Peptide

Each dry lyophilized PSM peptide stock was dissolved to a concentration of 10 mg/mL in a 1:1 mixture of hexafluoroisopropanol (HFIP) and trifluoroacetic acid (TFA) followed by a 5×20 s sonication with 30 s intervals using a probe sonicator (Biologics, Inc., Manassas, VA, USA) and incubation at room temperature for 1 h. Further, the stock was divided into aliquots, and the organic solvent was evaporated using speedvac (Scanvac, Labogene Aps, Allerød, Denmark) at 1000 rpm for 3 h at room temperature. Dried peptide stocks were stored at -80 °C prior to use.

4.3. Preparation of Lipid Vesicles

Dry LPS lipid was dissolved in MilliQ water to a concentration of 1 mg/mL. PE, DOPC and DOPG were dissolved in chloroform. Chloroform evaporated overnight in an exicator, and dry lipid was dissolved in MilliQ water. LPS, PE, DOPC and DOPG lipids were then frozen in liquid nitrogen and thawed in warm water 10 times. The extruder heating block (Avanti Polar Lipids, USA) was placed on a hot plate until temperature was at 37 °C. The sample was loaded into one of the gas-tight 1000 μ L glass syringes (Avanti Polar Lipids, USA) and put on the heating block to equilibrate for approx. 10 min. The sample was then passed through the extruder filter with a pore size of 0.1 μ m 15 times, and the resulting unilamellar vesicles were ready to use.

4.4. Preparation of Samples for Kinetic Experiments

ThT fluorescence was observed in clear-bottomed half-area 96-well black polystyrene microtiter plates (Corning, New York, NY, USA) with a non-binding surface. We used a Fluostar Omega (BMG Labtech, Ortenberg, Germany) plate reader in bottom-reading mode. Aliquots of purified PSMs were thawed and dissolved in dimethyl sulfoxide

(DMSO) to a concentration of 2 mg/mL prior to use. Concentrated peptide aliquots were diluted in MilliQ water and passed through a 0.22 μm filter. Lipid vesicles were added to the sample in different concentrations. ThT was added to the protein solutions to a final concentration of 40 μM . Further, samples were loaded (100 μL) in a 96-well plate and sealed to prevent evaporation. For each peptide, different concentrations—0.25 mg/mL (αPSM2 (110 μM) and αPSM4 (115 μM)) and 0.5 mg/mL (αPSM1 (222 μM) and αPSM3 (192 μM))—were used for kinetic measurements. The concentrations were chosen based on previous experiments made in the absence of lipids [35]. These concentrations allowed for observations of both acceleration and deceleration of the aggregation kinetics. The ThT:PSM peptide ratio was hence 1:6, 1:3, 1:5 and 1:3 for αPSM1 , αPSM2 , αPSM3 and αPSM4 , respectively. The plates were incubated at 37 $^{\circ}\text{C}$ under quiescent conditions, and ThT fluorescence was measured every 10 min (20 s for PSM α 3) with an excitation filter of 450 nm and an emission filter of 482 nm. The ThT fluorescence was followed for three repeats of each type of lipid concentration.

4.5. Far-UV Circular Dichroism (CD) Spectroscopy

At the end of ThT kinetics experiments, individual triplicate samples fibrillated in the absence and presence of high and low concentrations of DOPC, DOPG and LPS lipids were pooled. To remove the DMSO, samples were pelleted by centrifugation at 13,000 rpm for 30 min. The pellet was resuspended in the same volume of MilliQ followed by bath sonication. Samples were loaded in a 1 mm Quartz cuvette (Hellma, Müllheim, Germany).

CD was performed on a Chirascan Plus spectrophotometer (Applied Photophysics, Surrey, UK) at room temperature. Spectra were recorded between 185 and 250 nm with 1 nm bandwidth, step size of 0.5 nm, using three measurement repeats.

CD was performed on a JASCO-810 Spectrometer (Jasco, Oklahoma City, OK, USA) at 25 $^{\circ}\text{C}$, wavelength 190–250 nm, with a step size of 0.1 nm, 1 nm bandwidth, 5 measurement repeats. For each sample, correction for baseline contribution and the MilliQ signal were subtracted.

4.6. Fourier-Transform Infrared Spectroscopy

Fourier-transform infrared spectroscopy was recorded on a Tensor 27 FTIR instrument (Bruker Optics, Billerica, MA, USA) equipped with an attenuated total reflection accessory with a continuous flow of N_2 gas. To remove DMSO from the solution, fibrillated samples were centrifuged (13,000 rpm for 30 min), supernatants discarded and the pellet resuspended in MilliQ water. Prior to measurement, 5 μL samples were dried under a steam of N_2 gas, and 64 interferograms were accumulated with a spectral resolution of 2 cm^{-1} in the range of 1000–3998 cm^{-1} . OPUS 5.5 software (Bruker Optics, Billerica, MA, USA) was used to process the data, which included baseline subtraction, atmospheric compensation and a second derivative analysis. For comparative studies, all absorbance spectra were normalized. Only the amide I band in the range of 1600–1700 cm^{-1} comprising information about the secondary structure was shown.

4.7. Transmission Electron Microscopy

Fibrillated samples with and without lipid were collected following the ThT fibrillation kinetics assay by combining the contents of two to three identical wells from the plate. A 5 μL amount of all peptides with and without lipids was directly placed on a carbon-coated formvar grid (EM Resolutions, Keele, UK), allowed to adhere for 2 min and washed with MilliQ water followed by negative staining with 0.2% uranyl acetate for 2 min. Further, the grids were washed twice with MilliQ water and blotted dry using filter paper. The samples were examined using Morgani 268 (FEI Philips Electron microscope, Hillsboro, OR, USA) equipped with CCD digital camera with a resolution of 1376 \times 1032 and operated at an accelerating voltage of 80 KV.

Supplementary Materials: The supporting information can be downloaded at: <https://www.mdpi.com/article/10.3390/ijms25010102/s1>.

Author Contributions: Conceptualization, K.K. and M.A.; methodology, K.K. and K.H.H.; formal analysis, K.K. and M.A.; investigation, K.K. and K.H.H.; resources, M.A.; data curation, K.K.; writing—original draft preparation, K.K. and M.A.; writing—review and editing, K.K. and M.A.; visualization, K.K. and M.A.; supervision, M.A.; project administration, M.A.; funding acquisition, M.A. All authors have read and agreed to the published version of the manuscript.

Funding: This research was funded by the Department of Biomedicine, Aarhus University, Aarhus University Research Foundation AUFF-E-2017-7-16 and the L'Oréal and UNESCO for Women in Science national program.

Institutional Review Board Statement: Not applicable.

Informed Consent Statement: Not applicable.

Data Availability Statement: The data presented in this study are openly available at FigShare: https://figshare.com/articles/dataset/Differential_effects_of_lipid_bilayers_on_PSM_peptide_functional_amyloid_formation/24494953, accessed on 3 November 2023.

Conflicts of Interest: The authors declare no conflict of interest.

References

1. Maji, S.K.; Perrin, M.H.; Sawaya, M.R.; Jessberger, S.; Vadodaria, K.; Rissman, R.A.; Singru, P.S.; Nilsson, K.P.R.; Simon, R.; Schubert, D.; et al. Functional Amyloids as Natural Storage of Peptide Hormones in Pituitary Secretory Granules. *Science* **2009**, *325*, 328–332. [CrossRef]
2. Berson, J.F.; Theos, A.C.; Harper, D.C.; Tenza, D.; Raposo, G.; Marks, M.S. Proprotein Convertase Cleavage Liberates a Fibrillogenic Fragment of a Resident Glycoprotein to Initiate Melanosome Biogenesis. *J. Cell Biol.* **2003**, *161*, 521–533. [CrossRef]
3. Oh, J.; Kim, J.-G.; Jeon, E.; Yoo, C.-H.; Moon, J.S.; Rhee, S.; Hwang, I. Amyloidogenesis of Type III-Dependent Harpins from Plant Pathogenic Bacteria. *J. Biol. Chem.* **2007**, *282*, 13601–13609. [CrossRef]
4. Pham, C.L.L.; Kwan, A.H.; Sunde, M. Functional Amyloid: Widespread in Nature, Diverse in Purpose. *Essays Biochem.* **2014**, *56*, 207–219. [CrossRef]
5. Chapman, M.R.; Robinson, L.S.; Pinkner, J.S.; Roth, R.; Heuser, J.; Hammar, M.; Normark, S.; Hultgren, S.J. Role of *Escherichia coli* Curli Operons in Directing Amyloid Fiber Formation. *Science* **2002**, *295*, 851–855. [CrossRef]
6. Otzen, D.; Riek, R. Functional Amyloids. *Cold Spring Harb. Perspect. Biol.* **2019**, *11*, a033860. [CrossRef]
7. Romero, D.; Kolter, R. Functional Amyloids in Bacteria. *Int. Microbiol.* **2014**, *17*, 65–73. [CrossRef]
8. Wang, R.; Braughton, K.R.; Kretschmer, D.; Bach, T.-H.L.; Queck, S.Y.; Li, M.; Kennedy, A.D.; Dorward, D.W.; Klebanoff, S.J.; Peschel, A.; et al. Identification of Novel Cytolytic Peptides as Key Virulence Determinants for Community-Associated MRSA. *Nat. Med.* **2007**, *13*, 1510–1514. [CrossRef]
9. Schwartz, K.; Syed, A.K.; Stephenson, R.E.; Rickard, A.H.; Boles, B.R. Functional Amyloids Composed of Phenol Soluble Modulins Stabilize *Staphylococcus aureus* Biofilms. *PLoS Pathog.* **2012**, *8*, e1002744. [CrossRef]
10. Periasamy, S.; Joo, H.-S.; Duong, A.C.; Bach, T.-H.L.; Tan, V.Y.; Chatterjee, S.S.; Cheung, G.Y.C.; Otto, M. How *Staphylococcus aureus* Biofilms Develop Their Characteristic Structure. *Proc. Natl. Acad. Sci. USA* **2012**, *109*, 1281–1286. [CrossRef]
11. Salinas, N.; Colletier, J.-P.; Moshe, A.; Landau, M. Extreme Amyloid Polymorphism in *Staphylococcus aureus* Virulent PSM α Peptides. *Nat. Commun.* **2018**, *9*, 3512. [CrossRef]
12. Rayan, B.; Barnea, E.; Khokhlov, A.; Upcher, A.; Landau, M. Differential Fibril Morphologies and Thermostability Determine Functional Roles of *Staphylococcus aureus* PSM α 1 and PSM α 3. *Front. Mol. Biosci.* **2023**, *10*, 1184785. [CrossRef]
13. Salinas, N.; Tayeb-Fligelman, E.; Sammito, M.D.; Bloch, D.; Jelinek, R.; Noy, D.; Usón, I.; Landau, M. The Amphibian Antimicrobial Peptide Uperin 3.5 Is a Cross- α /Cross- β Chameleon Functional Amyloid. *Proc. Natl. Acad. Sci. USA* **2021**, *118*, e2014442118. [CrossRef]
14. Tayeb-Fligelman, E.; Salinas, N.; Tabachnikov, O.; Landau, M. *Staphylococcus aureus* PSM α 3 Cross- α Fibril Polymorphism and Determinants of Cytotoxicity. *Structure* **2020**, *28*, 301–313.e6. [CrossRef]
15. Tayeb-Fligelman, E.; Tabachnikov, O.; Moshe, A.; Goldshmidt-Tran, O.; Sawaya, M.R.; Coquelle, N.; Colletier, J.-P.; Landau, M. The Cytotoxic *Staphylococcus aureus* PSM α 3 Reveals a Cross- α Amyloid-like Fibril. *Science* **2017**, *355*, 831–833. [CrossRef]
16. Laabei, M.; Jamieson, W.D.; Yang, Y.; van den Elsen, J.; Jenkins, A.T.A. Investigating the Lytic Activity and Structural Properties of *Staphylococcus aureus* Phenol Soluble Modulin (PSM) Peptide Toxins. *Biochim. Biophys. Acta* **2014**, *1838*, 3153–3161. [CrossRef]
17. Surewaard, B.G.J.; de Haas, C.J.C.; Vervoort, F.; Rigby, K.M.; DeLeo, F.R.; Otto, M.; van Strijp, J.A.G.; Nijland, R. Staphylococcal Alpha-Phenol Soluble Modulins Contribute to Neutrophil Lysis after Phagocytosis. *Cell. Microbiol.* **2013**, *15*, 1427–1437. [CrossRef]
18. Kretschmer, D.; Gleske, A.-K.; Rautenberg, M.; Wang, R.; Köberle, M.; Bohn, E.; Schöneberg, T.; Rabiet, M.-J.; Boulay, F.; Klebanoff, S.J.; et al. Human Formyl Peptide Receptor 2 Senses Highly Pathogenic *Staphylococcus aureus*. *Cell Host Microbe* **2010**, *7*, 463–473. [CrossRef]

19. Joo, H.-S.; Cheung, G.Y.C.; Otto, M. Antimicrobial Activity of Community-Associated Methicillin-Resistant *Staphylococcus aureus* Is Caused by Phenol-Soluble Modulins. *J. Biol. Chem.* **2011**, *286*, 8933–8940. [\[CrossRef\]](#)
20. Cheung, G.Y.C.; Duong, A.C.; Otto, M. Direct and Synergistic Hemolysis Caused by Staphylococcus Phenol-Soluble Modulins: Implications for Diagnosis and Pathogenesis. *Microbes Infect.* **2012**, *14*, 380–386. [\[CrossRef\]](#)
21. Kizaki, H.; Omae, Y.; Tabuchi, F.; Saito, Y.; Sekimizu, K.; Kaito, C. Cell-Surface Phenol Soluble Modulins Regulate *Staphylococcus aureus* Colony Spreading. *PLoS ONE* **2016**, *11*, e0164523. [\[CrossRef\]](#) [\[PubMed\]](#)
22. Voyich, J.M.; Braughton, K.R.; Sturdevant, D.E.; Whitney, A.R.; Saïd-Salim, B.; Porcella, S.F.; Long, R.D.; Dorward, D.W.; Gardner, D.J.; Kreiswirth, B.N.; et al. Insights into Mechanisms Used by *Staphylococcus aureus* to Avoid Destruction by Human Neutrophils. *J. Immunol.* **2005**, *175*, 3907–3919. [\[CrossRef\]](#) [\[PubMed\]](#)
23. Geiger, T.; Francois, P.; Liebeke, M.; Fraunholz, M.; Goerke, C.; Krismer, B.; Schrenzel, J.; Lalk, M.; Wolz, C. The Stringent Response of *Staphylococcus aureus* and Its Impact on Survival after Phagocytosis through the Induction of Intracellular PSMs Expression. *PLoS Pathog.* **2012**, *8*, e1003016. [\[CrossRef\]](#) [\[PubMed\]](#)
24. Marinelli, P.; Pallares, I.; Navarro, S.; Ventura, S. Dissecting the Contribution of *Staphylococcus aureus* α -Phenol-Soluble Modulins to Biofilm Amyloid Structure. *Sci. Rep.* **2016**, *6*, 34552. [\[CrossRef\]](#) [\[PubMed\]](#)
25. Otto, M. Phenol-Soluble Modulins. *Int. J. Med. Microbiol. IJMM* **2014**, *304*, 164–169. [\[CrossRef\]](#) [\[PubMed\]](#)
26. Cheung, G.Y.C.; Kretschmer, D.; Queck, S.Y.; Joo, H.-S.; Wang, R.; Duong, A.C.; Nguyen, T.H.; Bach, T.-H.L.; Porter, A.R.; DeLeo, F.R.; et al. Insight into Structure-Function Relationship in Phenol-Soluble Modulins Using an Alanine Screen of the Phenol-Soluble Modulin (PSM) A3 Peptide. *FASEB J.* **2014**, *28*, 153–161. [\[CrossRef\]](#) [\[PubMed\]](#)
27. Landau, M. Beyond One-Trick Ponies: The Multifunctional Marvels of Microbial Functional Amyloids. *Microorganisms* **2023**, *11*, 1201. [\[CrossRef\]](#)
28. Surewaard, B.G.J.; Nijland, R.; Spaan, A.N.; Kruijtz, J.A.W.; de Haas, C.J.C.; van Strijp, J.A.G. Inactivation of Staphylococcal Phenol Soluble Modulins by Serum Lipoprotein Particles. *PLoS Pathog.* **2012**, *8*, e1002606. [\[CrossRef\]](#)
29. Hommes, J.W.; Kratoch, R.M.; Wahlen, S.; de Haas, C.J.C.; Hildebrand, R.B.; Hovingh, G.K.; Otto, M.; van Eck, M.; Hoekstra, M.; Korpmaal, S.J.A.; et al. High Density Lipoproteins Mediate in Vivo Protection against Staphylococcal Phenol-Soluble Modulins. *Sci. Rep.* **2021**, *11*, 15357. [\[CrossRef\]](#)
30. Swasthi, H.M.; Mukhopadhyay, S. Electrostatic Lipid-Protein Interactions Sequester the Curli Amyloid Fold on the Lipopolysaccharide Membrane Surface. *J. Biol. Chem.* **2017**, *292*, 19861–19872. [\[CrossRef\]](#)
31. Najarzadeh, Z.; Pedersen, J.N.; Christiansen, G.; Shojaosadati, S.A.; Pedersen, J.S.; Otzen, D.E. Bacterial Amphiphiles as Amyloid Inducers: Effect of Rhamnolipid and Lipopolysaccharide on FapC Fibrillation. *Biochim. Biophys. Acta BBA-Proteins Proteom.* **2019**, *1867*, 140263. [\[CrossRef\]](#) [\[PubMed\]](#)
32. Galvagnion, C.; Brown, J.W.P.; Ouberaï, M.M.; Flagmeier, P.; Vendruscolo, M.; Buell, A.K.; Sparr, E.; Dobson, C.M. Chemical Properties of Lipids Strongly Affect the Kinetics of the Membrane-Induced Aggregation of α -Synuclein. *Proc. Natl. Acad. Sci. USA* **2016**, *113*, 7065–7070. [\[CrossRef\]](#) [\[PubMed\]](#)
33. Bartels, T.; Ahlstrom, L.S.; Leftin, A.; Kamp, F.; Haass, C.; Brown, M.F.; Beyer, K. The N-Terminus of the Intrinsically Disordered Protein α -Synuclein Triggers Membrane Binding and Helix Folding. *Biophys. J.* **2010**, *99*, 2116–2124. [\[CrossRef\]](#) [\[PubMed\]](#)
34. LeVine, H. Thioflavine T Interaction with Synthetic Alzheimer's Disease Beta-Amyloid Peptides: Detection of Amyloid Aggregation in Solution. *Protein Sci. Publ. Protein Soc.* **1993**, *2*, 404–410. [\[CrossRef\]](#) [\[PubMed\]](#)
35. Zaman, M.; Andreasen, M. Cross-Talk between Individual Phenol-Soluble Modulins in *Staphylococcus aureus* Biofilm Enables Rapid and Efficient Amyloid Formation. *eLife* **2020**, *9*, e59776. [\[CrossRef\]](#) [\[PubMed\]](#)
36. Faller, P.; Hureau, C. Reproducibility Problems of Amyloid- β Self-Assembly and How to Deal with Them. *Front. Chem.* **2020**, *8*, 611227. [\[CrossRef\]](#) [\[PubMed\]](#)
37. Meisl, G.; Kirkegaard, J.B.; Arosio, P.; Michaels, T.C.T.; Vendruscolo, M.; Dobson, C.M.; Linse, S.; Knowles, T.P.J. Molecular Mechanisms of Protein Aggregation from Global Fitting of Kinetic Models. *Nat. Protoc.* **2016**, *11*, 252–272. [\[CrossRef\]](#)
38. Cohen, S.I.A.; Linse, S.; Luheshi, L.M.; Hellstrand, E.; White, D.A.; Rajah, L.; Otzen, D.E.; Vendruscolo, M.; Dobson, C.M.; Knowles, T.P.J. Proliferation of Amyloid-B42 Aggregates Occurs through a Secondary Nucleation Mechanism. *Proc. Natl. Acad. Sci. USA* **2013**, *110*, 9758–9763. [\[CrossRef\]](#)
39. Collins, S.R.; Douglass, A.; Vale, R.D.; Weissman, J.S. Mechanism of Prion Propagation: Amyloid Growth Occurs by Monomer Addition. *PLoS Biol.* **2004**, *2*, e321. [\[CrossRef\]](#)
40. Meisl, G.; Yang, X.; Hellstrand, E.; Frohm, B.; Kirkegaard, J.B.; Cohen, S.I.A.; Dobson, C.M.; Linse, S.; Knowles, T.P.J. Differences in Nucleation Behavior Underlie the Contrasting Aggregation Kinetics of the A β 40 and A β 42 Peptides. *Proc. Natl. Acad. Sci. USA* **2014**, *111*, 9384–9389. [\[CrossRef\]](#)
41. Munke, A.; Persson, J.; Weiffert, T.; De Genst, E.; Meisl, G.; Arosio, P.; Carnerup, A.; Dobson, C.M.; Vendruscolo, M.; Knowles, T.P.J.; et al. Phage Display and Kinetic Selection of Antibodies That Specifically Inhibit Amyloid Self-Replication. *Proc. Natl. Acad. Sci. USA* **2017**, *114*, 6444–6449. [\[CrossRef\]](#) [\[PubMed\]](#)
42. Månsson, C.; Arosio, P.; Hussein, R.; Kampinga, H.H.; Hashem, R.M.; Boelens, W.C.; Dobson, C.M.; Knowles, T.P.J.; Linse, S.; Emanuelsson, C. Interaction of the Molecular Chaperone DNAJB6 with Growing Amyloid-Beta 42 (A β 42) Aggregates Leads to Sub-Stoichiometric Inhibition of Amyloid Formation. *J. Biol. Chem.* **2014**, *289*, 31066–31076. [\[CrossRef\]](#) [\[PubMed\]](#)

43. Michaels, T.C.T.; Šarić, A.; Meisl, G.; Heller, G.T.; Curk, S.; Arosio, P.; Linse, S.; Dobson, C.M.; Vendruscolo, M.; Knowles, T.P.J. Thermodynamic and Kinetic Design Principles for Amyloid-Aggregation Inhibitors. *Proc. Natl. Acad. Sci. USA* **2020**, *117*, 24251–24257. [[CrossRef](#)] [[PubMed](#)]
44. Najarzadeh, Z.; Zaman, M.; Sereikaite, V.; Strømgaard, K.; Andreassen, M.; Otzen, D.E. Heparin Promotes Fibrillation of Most Phenol-Soluble Modulin Virulence Peptides from *Staphylococcus aureus*. *J. Biol. Chem.* **2021**, *297*, 100953. [[CrossRef](#)] [[PubMed](#)]
45. Otzen, D. Protein-Surfactant Interactions: A Tale of Many States. *Biochim. Biophys. Acta* **2011**, *1814*, 562–591. [[CrossRef](#)]
46. Fersht, A. *Structure and Mechanism in Protein Science: A Guide to Enzyme Catalysis and Protein Folding*; Freeman Co.: New York, NY, USA, 1999.
47. Bertani, B.; Ruiz, N. Function and Biogenesis of Lipopolysaccharides. *EcoSal Plus* **2018**, *8*, 1110–1128. [[CrossRef](#)]
48. Rajagopal, M.; Walker, S. Envelope Structures of Gram-Positive Bacteria. *Curr. Top. Microbiol. Immunol.* **2017**, *404*, 1–44. [[CrossRef](#)]
49. Malishev, R.; Tayeb-Fligelman, E.; David, S.; Meijler, M.M.; Landau, M.; Jelinek, R. Reciprocal Interactions between Membrane Bilayers and *S. Aureus* PSM α 3 Cross- α Amyloid Fibrils Account for Species-Specific Cytotoxicity. *J. Mol. Biol.* **2018**, *430*, 1431–1441. [[CrossRef](#)]

Disclaimer/Publisher’s Note: The statements, opinions and data contained in all publications are solely those of the individual author(s) and contributor(s) and not of MDPI and/or the editor(s). MDPI and/or the editor(s) disclaim responsibility for any injury to people or property resulting from any ideas, methods, instructions or products referred to in the content.